

# Adsorption of Fibronectin, Fibrinogen, and Albumin on TiO<sub>2</sub>: Time-Resolved Kinetics, Structural Changes, and Competition Study

Marta Pegueroles · Chiara Tonda-Turo ·  
Josep A. Planell · Francisco-Javier Gil ·  
Conrado Aparicio

Received: 19 June 2012 / Accepted: 18 July 2012 / Published online: 9 August 2012  
© The Author(s) 2012. This article is published with open access at Springerlink.com

**Abstract** An understanding of protein adsorption process is crucial for designing biomaterial surfaces. In this work, with the use of a quartz-crystal microbalance with dissipation monitoring, we researched the following: (a) the kinetics of adsorption on TiO<sub>2</sub> surfaces of three extensively described proteins that are relevant for metallic implant integration [i.e., albumin (BSA), fibrinogen (Fbg), and

fibronectin (Fn)]; and (b) the competition of those proteins for adsorbing on TiO<sub>2</sub> in a two-step experiment consisted of sequentially exposing the surfaces to different mono-protein solutions. Each protein showed a different process of adsorption and properties of the adlayer—calculated using the Voigt model. The competition experiments showed that BSA displaced larger proteins such as Fn and Fbg when BSA was introduced as the second protein in the system, whereas the larger proteins laid on top of BSA forming an adsorbed protein bi-layer when those were introduced secondly in the system.

M. Pegueroles · C. Tonda-Turo · J. A. Planell · F.-J. Gil ·  
C. Aparicio  
Biomaterials, Biomechanics, and Tissue Engineering Group,  
Department of Material Science and Metallurgy, Technical  
University of Catalonia, Av. Diagonal 647,  
08028 Barcelona, Spain  
e-mail: marta.pegueroles@upc.edu

C. Tonda-Turo  
e-mail: chiara.tondaturo@polito.it

J. A. Planell  
e-mail: japlanell@ibec.pcb.ub.es; josep.a.planell@upc.edu

F.-J. Gil  
e-mail: francesc.xavier.gil@upc.edu

M. Pegueroles · J. A. Planell · F.-J. Gil  
Biomedical Research Networking Centre in Bioengineering,  
Biomaterials and Nanomedicine (CIBER-BBN),  
E50118 Zaragoza, Spain

J. A. Planell  
Institute for Bioengineering of Catalonia (IBEC),  
Baldiri Reixac 13, 08028 Barcelona, Spain

## Present Address:

C. Aparicio (✉)  
Department of Restorative Sciences, School of Dentistry,  
Minnesota Dental Research Center for Biomaterials and  
Biomechanics (MDRCBB), University of Minnesota,  
16-212 Moos Tower, 515 Delaware St. S.E., Minneapolis,  
MN 55455, USA  
e-mail: apari003@umn.edu

## 1 Introduction

The first event taking place at the biomaterial-tissue interface is the interaction of water molecules and salt ions with the surface of the implant. Shortly after the formation of the hydration layer, blood proteins start to crowd the biomaterial surface [1, 2]. Eventually, those proteins form a layer on top of the implanted material. When cells reach the implant surface, they scan the layer of proteins looking for activation factors to attach to that surface and react accordingly. Thus, protein adsorption on biomaterial surfaces plays a crucial role in the integration of an implant in the human body.

Ideally, the surface properties of the implantable material will trigger appropriate responses for specific applications by controlling the type, amount, and conformation of the proteins that will adsorb on the implant. Understanding the process of protein adsorption is then crucial to the surface design of biomaterials.

Proteins are a special, highly complex, and important case of particles adsorbing at surfaces. Protein adsorption is a dynamic process involving non-covalent interactions

such as hydrophobic interactions, electrostatic forces, hydrogen bonding and van der Waals' forces [3]. On the one side, the non-covalent interactions are controlled by multiple protein parameters, such as protein size, pI, secondary and tertiary structure [4, 5]. On the other side, surface properties such as surface energy, roughness and chemistry have been also identified as key factors influencing the process of protein adsorption [4, 6–8].

Protein adsorption to surfaces is the first step in many fundamental biological processes such as blood coagulation cascade and trans-membrane signalling [4]. There are multiple proteins in human blood plasma. Among them, fibrinogen (Fbg), fibronectin (Fn) and albumin (Alb) which constitute a set of well-known, thoroughly characterized, extensively described proteins [9]. Several studies have suggested that platelet adhesion and activation might be particularly affected by adsorbed fibrinogen, a mediator of platelet activation via its direct interaction with platelet receptors [10–12]. Fibronectin is a key component of the extracellular matrix (ECM), is a large dimeric glycoprotein triggering cell adhesion [13], undergoes cell-driven assembly in supramolecular fibrils, and provides specific binding sites for various ECM biopolymers [14]. Albumin is the most abundant component of many biofluids, serving as transport media for various metabolites and as regulator of osmotic pressure [14, 15]. Moreover, albumin is a widespread protein used to block 'non-specific' cell adhesion [16], but some controversy exists given that albumin has been found to promote platelet and macrophage adhesion [17, 18].

Metal surfaces are, with few exceptions, covered with a metallic oxide layer of a few to several nanometers in thickness. As a consequence, interactions between metal implants, proteins, and cells are governed by the physical–chemical properties of their corresponding metallic oxides. The excellent chemical inertness, corrosion resistance, re-passivation ability, and biocompatibility of titanium are thought to result from the chemical stability (high corrosion resistance) a thermodynamically stable state and structure of the titanium oxide film mainly composed of  $\text{TiO}_2$  at physiological pH values [19–22]. The following crystal structures have been recognized for  $\text{TiO}_2$ : rutile (tetragonal), anatase (tetragonal), and brookite (orthorhombic).  $\text{TiO}_2$  also exists in an amorphous state [23]. Regarding the surface oxide layer on c.p. Ti dental implant systems, spectroscopic studies suggest that the oxide is amorphous and its thickness is approximately 2–17 nm [22–24].

In vitro studies have shown that material surface properties, including the negatively charged and hydrophilic  $\text{TiO}_2$  layer, are of importance for protein adsorption [25]. One reported issue is that in vitro adsorption of the same protein on the same type of surface may vary considerably

between different studies as a consequence of the different experimental conditions. However, some general characteristics of protein interaction with titanium surfaces can be found. Proteins in solution accumulate spontaneously at materials interfaces and, in the case of titanium surfaces, most of them adsorb irreversibly since the process is highly energetically favorable [26]. However, some adsorbed proteins can detach due to protein competition and displacement processes [26]. The replacement of initially adsorbed proteins with high mobility by new proteins with lower mobility but higher affinity for the surface is the so-called Vroman effect [4]. Different adsorption isotherms reported in the literature [1, 27, 28] showed high affinity of fibronectin to titanium surfaces.

Proteins systems are very complex and thus, measurements with well-defined model systems carried out under well-controlled conditions are essential to understand the underlying mechanisms of protein adsorption [29]. Different techniques have been used for quantitatively characterize protein adsorption on solid surfaces. Most of them either (a) rely on labelling adsorbing molecules with a radioactive or fluorescent tag and comparing their signal on the surface before and after adsorption or (b) are based in changes in the optical properties of the surface while the layer of proteins is being adsorbed, such as ellipsometry and surface plasmon resonance. The former are laborious procedures that do not allow real-time monitoring of the studied process. The later provides us with real-time data of the formation of the protein layer; however, information of the structural/conformational changes of the protein layer is not obtained. We used a quartz-crystal microbalance with dissipation monitoring (QCM-D). With QCM-D the kinetics of both mass changes and structural/mechanical properties changes are obtained [30–32]. This is possible because the equipment simultaneously collects both the resonant frequency and the energy dissipation signals of a quartz crystal sensor coated with the material in question. The change in mass of the sensor while the proteins adsorb produces changes in the frequency of the sensor. Also, the structural and conformational effects at the protein layer when water incorporates into and interacts with the protein layer can be monitored by tracking changes in the energy dissipation of the system [33]. However, the specific structural changes have to be further investigated with complementary experimental techniques.

Even though increasing number of studies have investigated the process of protein adsorption on biomaterials there is still lack of fundamental knowledge on how some specific combinations of relevant proteins interact with synthetic substrates of clinical interest. We report here on (a) the kinetics of the protein adsorption process, (i.e. evolution of mass and structure of the protein layer on sensors coated with  $\text{TiO}_2$  from three different monopro-

solutions, Fbg, Fn, and Alb) and (b) the competition of the proteins for adsorbing on the TiO<sub>2</sub> surfaces in two-step experiments; (i.e. sequentially exposing the surfaces to two different monoproduct solutions). All those experiments were performed using QCM-D.

## 2 Materials and Methods

### 2.1 Materials

#### 2.1.1 TiO<sub>2</sub>-Coated Sensors

Titanium QCM-D sensors (QSX 310) were purchased at Q-Sense (Sweden). The sensors consisted of gold-coated quartz crystals (14 mm in diameter) covered using vapour deposition with a 50-nm thick TiO<sub>2</sub> layer. The fundamental mode of the sensors was at 4.95 MHz. The cleaning protocol used before starting each experiment was: (1) 10 min sonication with ethanol (96 %, Panreac); (2) 10 min sonication with acetone (99.5 %, Panreac); (3) 10 min sonication with MilliQ<sup>®</sup> ultrapure water; and (4) 10 min UV/ozone chamber (BioForce Nanosciences, Ames, USA). During the cleaning process the sensors were held on a Teflon<sup>®</sup> Q-Sense Sensor Holder.

#### 2.1.2 Protein Solutions

Human fibronectin (Fn, ≥95 %, CAS Number: 86088-83-7), human fibrinogen (Fbg, 50–70 %, CAS Number: 9001-32-5) and bovine serum albumin (BSA, ≥96 %, CAS Number: 9048-46-8) were purchased at Sigma Aldrich (Saint Louis, USA). The protein concentration of each solution was different depending on the type of protein and the specific test (see below).

### 2.2 Methods

#### 2.2.1 Surface Characterization of TiO<sub>2</sub>-Coated Sensors

Roughness and wettability of TiO<sub>2</sub>-coated sensors (Q-Sense, Sweden) was measured.

Roughness measurements were performed with a white-light interferometer (Wyko NT1100, Veeco, USA). Images were taken using a 10× objective. A Gaussian filter was used to separate waviness and form from roughness of the surface by applying a cut-off value ( $\lambda_c$ ) of 0.25 mm according to ISO 11562:1996 standard [34].

The static contact angle (SCA) of the TiO<sub>2</sub>-coated sensors was assessed using the sessile drop method. Ultrapure distilled water (Millipore) 3–6 μl drops were generated with a micrometric syringe and deposited on the substrate surface. Syringe and sample were placed inside a

customized PMMA environmental chamber with two optical glass windows to saturate humidity during the experiments. The wettability studies were performed with a contact angle video based system (Contact Angle System OCA15plus, Dataphysics, Germany) and analysed with the SCA20 software (Dataphysics, Germany).

The chemical analysis of the TiO<sub>2</sub> surfaces was performed with a X-ray photoelectron spectrometer (XPS) XPS experiments were performed in a PHI 5500 Multi-technique System (Physical Electronics) with a monochromatic X-ray source (Aluminium K $\alpha$  line of 1,486.6 eV energy and 350 W), placed perpendicular to the analyzer axis (takeoff angle of 45°). The analyzed area was a circle of 0.8 mm diameter, and selected resolution for the fitted spectra was 23.5 eV of Pass Energy and 0.1 eV/step. The analysis of the spectra obtained was made with the software Multipak. All the binding energies were referenced to the C1 s peak at 284.8 eV.

Grazing incidence X-ray diffraction (GIXD) (D8 Advance, Bruker<sup>®</sup> Axs) was also carried out on TiO<sub>2</sub>-coated sensors. The diffractometer was operated at 40 kV and 10 mA using a Ni filter, Cu K $\alpha$  radiation, and was equipped with a 0.6 mm slit. The incidence angle was fixed at 1° thus limiting the X-ray beam penetration depth. A counting time of 8 s per 0.01° step was set for each measurement. A range of 2 $\theta$  angles of 10–80° were scanned.

#### 2.2.2 Protein Adsorption Tests

**2.2.2.1 Adsorption from Monoproduct Solutions** Adsorption of Fn, Fbg and BSA on TiO<sub>2</sub>-coated sensors from monoproduct solutions were performed at 37 °C. The kinetics of protein adsorption and the structural changes of the adlayer of proteins were studied with different protein-concentration solutions. The protein concentration of each solution was based on concentrations providing maximum levels of adsorbed protein per unit area at surface saturation [27, 35–38]:

- (a) Fibronectin [27, 36, 37]: 20–30–40–50 μg/ml
- (b) Fibrinogen [38]: 80–100 μg/ml
- (c) Bovine serum albumin [35]: 100 μg/ml

Only a concentration value was studied for BSA protein solutions since Hughes et al. [35] and Wassell et al. [35] showed a saturation value of 100 μg/ml for BSA protein on TiO<sub>2</sub> surfaces at pH 7.2.

**2.2.2.2 Two-Step Protein Adsorption** Two-step protein adsorption studies of Fn, Fbg and BSA on TiO<sub>2</sub>-coated sensors were performed at 37 °C. Two-step adsorption studies consisted of sequentially exposing the TiO<sub>2</sub> surfaces to two solutions with different proteins. These experiments aimed to study the processes of interaction

and/or competition between the two types of proteins as well as to assess the comparative affinity of the proteins for the studied surface. We studied 4 two-step protein sequences; i.e. BSA–Fn, BSA–Fbg, Fn–BSA and Fbg–BSA. The concentration of each protein in PBS 1× solution was established to match human blood plasma ratios [38–40]:

- (a) BSA–Fbg: 500 µg/ml for BSA and 50 µg/ml for Fbg
- (b) Fbg–BSA: 50 µg/ml for Fbg and 500 µg/ml for BSA
- (c) BSA–Fn: 2 mg/ml for BSA and 20 µg/ml for Fn
- (d) Fn–BSA: 50 µg/ml for Fn and 5 mg/ml for BSA

The first step of the experimental protocol consisted of introducing the first protein and studying its adsorption on TiO<sub>2</sub> surfaces. Then, when the frequency and the dissipation shift reached the stable point (as previously defined), the crystal surface with the initial layer of proteins was cleaned. PBS was introduced in the system to remove/wash the reversibly adsorbed proteins on the surface. Finally, the second step consisted of introducing in the QCM-D sensor chamber the second protein in solution until the new adlayer reached the stable point.

### 2.2.3 Quartz Crystal Microbalance with Dissipation Monitoring

The QCM-D is a sensitive tool for the study of the kinetics of protein adsorption [41, 42] as well as other surface-related processes like gas adsorption and reactions on surfaces in the monolayer and sub-monolayer regimes [43]. A quartz crystal microbalance consists of a piezoelectric quartz crystal sensor that is excited to oscillation at its fundamental resonant frequency,  $f$ . The equipment is used to measure very small masses added on the surface of the sensor because an increase in mass ( $\Delta m$ ) bound to the quartz surface causes the crystal oscillation frequency to decrease, obtaining a negative shift of the resonance frequency ( $-\Delta f$ ). The linear relation between  $\Delta m$  and  $\Delta f$  was demonstrated in 1959 by Sauerbrey [33, 44]

$$df = \Delta f = -\frac{f_q}{t_q \cdot \rho_q} \cdot \Delta m = -n \cdot \frac{1}{C} \cdot \Delta m \quad (1)$$

where  $f_q$  is the resonant frequency in vacuum of the quartz plate, its thickness  $t_q$ , and its density  $\rho_q$ .  $C$  is the mass sensitivity constant ( $C = 17.7 \text{ ng cm}^{-2} \text{ Hz}^{-1}$  at 5 MHz) and  $n$  is the overtone number ( $n = 1, 3, \dots$ ).

Equation 1 holds if the adsorbed layer is rigid, if the added mass is small compared to the weight of the crystal, if there is no slip in the metal/layer interface, and if the layer is homogeneously distributed on the surface. The Sauerbrey relation concludes that the change in resonance frequency is proportional to the change in the adsorbed mass if the adsorbed layer is much smaller than the mass of the crystal [44].

In other situations, where the layer is not rigid and/or too thick, the response of the QCM is more complex because the Sauerbrey relation ‘fails’. A viscoelastic or thick layer constitutes a coupled oscillator for which  $\Delta f$  is not directly proportional to  $\Delta m$ , i.e. the effectively coupled mass depends on how the oscillatory motion of the crystal propagates into and through the viscoelastic adlayer [45]. In addition to that, most surface-adsorbed protein layers are hydrated, so they are not only highly viscous and cause significant energy dissipation, but also add mass to the adsorbed protein layer. In those cases the dissipation factor,  $D$ , simultaneously calculated with  $f$  when using the QCM must also be taken into consideration [44, 46]. The dissipation factor is inversely proportional to the Q-factor of the oscillator [32], which is a nondimensional parameter that compares the time constant for decay of an oscillating physical system’s amplitude to its oscillation period as defined by:

$$D = \frac{1}{Q} = \frac{E_{\text{dissipated}}}{2 \cdot \pi \cdot E_{\text{stored}}} \quad (2)$$

where  $E_{\text{dissipated}}$  is the energy dissipated during one period of oscillation, and  $E_{\text{stored}}$  is the energy stored in the oscillating system.

### 2.2.4 QCM-D Data Analysis

A time-resolved analysis of  $f$  and  $D$  shifts for the different overtones is required to assess the model to be used. Under normal conditions, the fundamental overtone is disregarded since it is too sensitive; whereas the third, fifth and seventh overtone are studied. The data will require viscoelastic modelling if  $D$  values are not close to zero, or if  $D$ -shifts (in  $1\text{E}-6$ ) are higher than 5 % of  $f$  shifts (in Hz). In addition, if there are significant differences between overtones, viscoelastic modelling is suggested [47].

A viscoelastic adlayer in all surfaces reported here was assessed and consequently analyzed. For modelling the adsorbed layer of proteins we have used the so-called Voigt-based representation of a viscoelastic solid, in which the adsorbed film is represented by a (frequency dependant) complex shear modulus. The description of the model and details on its implementation using a QCM-D are reported elsewhere [31]. The calculation of the relevant parameters from the obtained protein layer, i.e. viscosity, shear elastic modulus and thickness, according to the Voigt model was performed with the appropriate software (Qtools, Q-Sense AB, Sweden). To do so, we initially fixed two parameters (fluid density and fluid viscosity) to those corresponding to water. This is a good estimation since the system includes a highly hydrated protein film. The density of the protein layer, also fixed to fit the model, might vary between  $1,000 \text{ kg/m}^3$  (water) and  $1,350 \text{ kg/m}^3$  (protein)

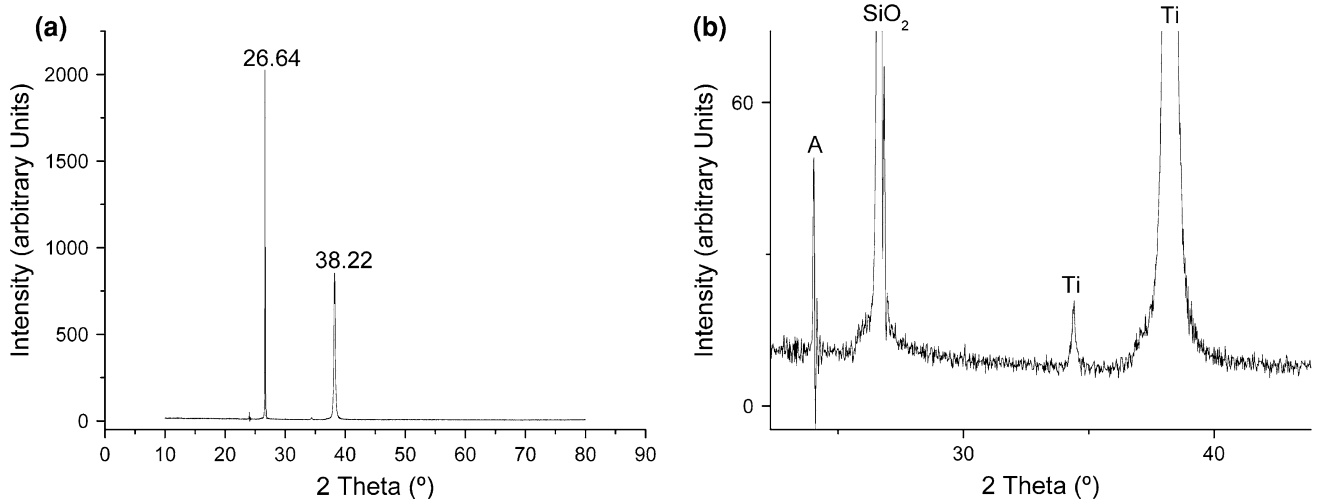


**Fig. 1** **a** Grazing incidence X-ray diffraction pattern of a TiO<sub>2</sub>-coated QCM-D sensor. **b** Enlarged view of the  $2\theta = 23\text{--}44^\circ$  region of the pattern in (a). A: anatase-TiO<sub>2</sub>; Ti: titanium; SiO<sub>2</sub>: quartz

[32, 48–50] depending on protein coverage. 1,200 kg/m<sup>3</sup> was chosen on the basis that a saturated protein coverage is slightly above 50 % [32, 48, 50]. The rest of the protein layer should be covered by water.

### 3 Results

#### 3.1 Surface Characterization of TiO<sub>2</sub>-Coated Sensors

XPS revealed the presence of O, C, N and Ti at the TiO<sub>2</sub>-surface of the sensor with a 2.31 O/Ti ratio. Figure 1 shows grazing incidence X-ray diffraction (GIXD) patterns of the TiO<sub>2</sub>-coated sensors. Diffraction peaks for titanium, quartz, and TiO<sub>2</sub> in anatase structure were detected (JCPDS-International Centre for Diffraction Data cards no. 21-1272 for anatase, no. 21-1276 for rutile, no. 44-1294 for titanium, and no. 46-1045 for SiO<sub>2</sub>, quartz).

The arithmetic mean value  $\pm$  standard deviation of the roughness,  $R_a$ , for the TiO<sub>2</sub> surfaces was  $5.11 \pm 0.31$  nm; and the mean static water  $\pm$  standard deviation contact angle was  $51.25 \pm 2.87^\circ$ .

##### 3.1.1 Adsorption from Monoprotein Solutions

Figure 2 shows changes in  $f$  (left) and  $D$  (right) as a function of time during adsorption of Fn, Fbg, and BSA on TiO<sub>2</sub>-coated sensors from solutions with all the different protein concentrations tested. The adsorption kinetics for all the proteins tested followed a similar pattern consisting of a rapid frequency decrease—mass increase—followed by a slower decrease. A stable point for the adsorption process was defined as frequency shift variation  $<1$  %/min. As expected, the higher the concentration for the same protein

in solution, the lower the value of frequency at the stable point and thus, the higher the mass adsorbed at the TiO<sub>2</sub> surface.  $D$  increased with time, which demonstrated that more energy was dissipated in the adlayer as more proteins were adsorbed; however, the kinetics for the shift in frequency and energy dissipation did not match. Figure 3 shows one representative  $\Delta f$  versus  $\Delta D$  plot for the adsorption process of each protein studied; 40, 100, 100  $\mu\text{g/ml}$  concentration of Fn, Fbg, and BSA, respectively. Figure 3 eliminates time as an explicit parameter. The slope of the  $\Delta f$  versus  $\Delta D$  plot was constant for the whole experiment during Fn adsorption on TiO<sub>2</sub>-coated sensors. However, the slope changed at different points during adsorption of both Fbg and BSA. The changes in slope of the  $\Delta f$  versus  $\Delta D$  plot have been related to different stages/phases in the conformational state of the adlayer formed [33].

Viscosity, thickness, elastic shear modulus, and surface mass density of the adlayer formed during experiments presented in Fig. 3 are shown in Fig. 4. All those properties were calculated using the Voigt model. Fbg adsorption yielded the thickest layer and the highest surface mass density for these specific experimental conditions of the three proteins tested. BSA adsorption on TiO<sub>2</sub> yielded a noticeable thinner and less dense layer compared to the one obtained with Fn and Fbg (Fig. 4a, b). Fn adsorption resulted in the most rigid and viscous adlayer of the three proteins tested.

#### 3.2 Two-Step Protein Adsorption

Figures 5, 6 and 7 show results for two-step protein adsorption studies where a first protein was introduced in the system and adsorbed on the surface; followed by PBS cleanings that were detected by sudden big changes in

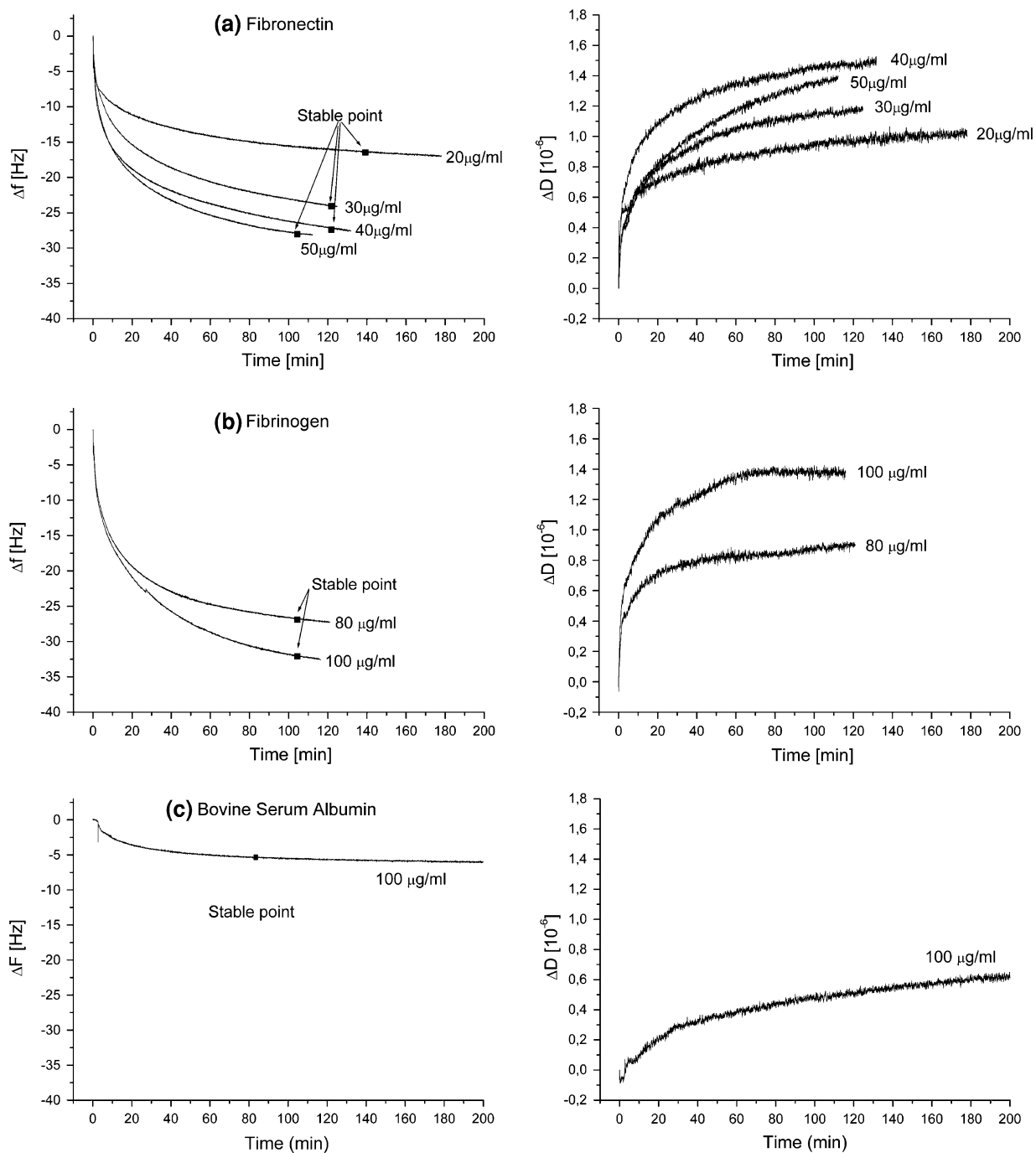


**Fig. 2** Frequency (*left*) and dissipation (*right*) shift versus time plots of adsorbed protein layers on  $\text{TiO}_2$ -coated crystals. From **a** 20, 30, 40 and 50  $\mu\text{g/ml}$  Fn solutions; **b** 80 and 100  $\mu\text{g/ml}$  Fbg solutions; and **c** 100  $\mu\text{g/ml}$  BSA solution

frequency; and final introduction of the second protein in the system to compete for adsorption on the surface.

### 3.2.1 Interactions Between BSA and Fbg on $\text{TiO}_2$

First step: solution with BSA—Second step: solution with Fbg (BSA–Fbg).

Figure 5 shows time-resolved frequency and dissipation shift graphs during the two-step BSA–Fbg protein adsorption process. BSA adsorption caused a final  $\Delta f = -12$  Hz; then, the addition of Fbg increased the frequency shift of the studied system to a final value of  $-18$  Hz. The  $\Delta D$  versus  $t$  graph showed a continuous increase in energy dissipation during BSA adsorption followed by additional

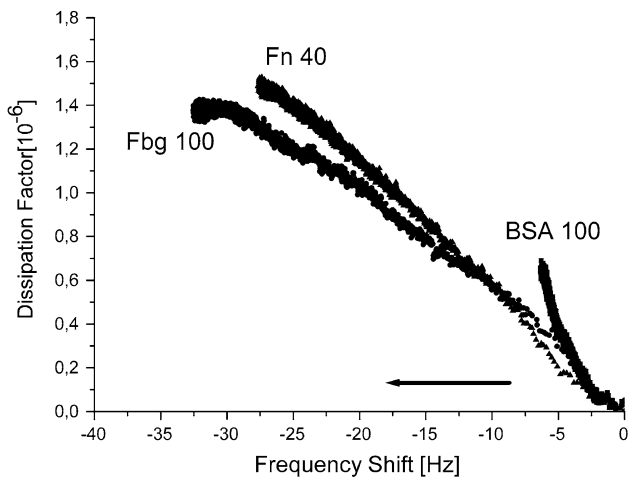


**Fig. 3**  $\Delta D$  versus  $\Delta f$  plots for the adsorption of Fn (40  $\mu\text{g/ml}$ ), Fbg (100  $\mu\text{g/ml}$ ) and BSA (100  $\mu\text{g/ml}$ ) on  $\text{TiO}_2$ -coated sensors. The arrow shows the direction from the initial to the final point of the experiments

increase during the first 20 min of Fbg adsorption up to a steady value that indicated saturation of the layer of proteins.

Figure 5b shows the  $\Delta D$  versus  $\Delta f$  plot for the experiment presented in Fig. 5a. The process of BSA adsorption showed a similar response than the one obtained for the one-step adsorption from monoprotein solutions (Fig. 3), where three different slopes/phases were detected. These phases had increasing  $\Delta D/\Delta f$  slope for increasing  $\Delta D$ . That indicated an ongoing decrease of the shear elastic modulus of the adlayer during the process of BSA adsorption on the  $\text{TiO}_2$ -surfaces. Further Fbg adsorption on the BSA layer also showed the same type of response than in the case of the adsorption from a one-step Fbg solution (Fig. 3); i.e., two slopes/phases and final near zero  $\Delta D/\Delta f$  slope values.

First step: solution with Fbg—Second step: solution with BSA (Fbg–BSA).

Figure 5 a reports on frequency and dissipation shift versus time during the two-step protein adsorption process of BSA–Fbg solutions in PBS. During adsorption of Fbg on  $\text{TiO}_2$ -coated sensors a rapid and significant decrease of frequency of the sensor was coupled with a continuous increase of the dissipation shift. Interestingly, the further exposure of the Fbg-coated  $\text{TiO}_2$ -surface to the BSA solution caused a continuous increase of  $\Delta f$ —decrease of

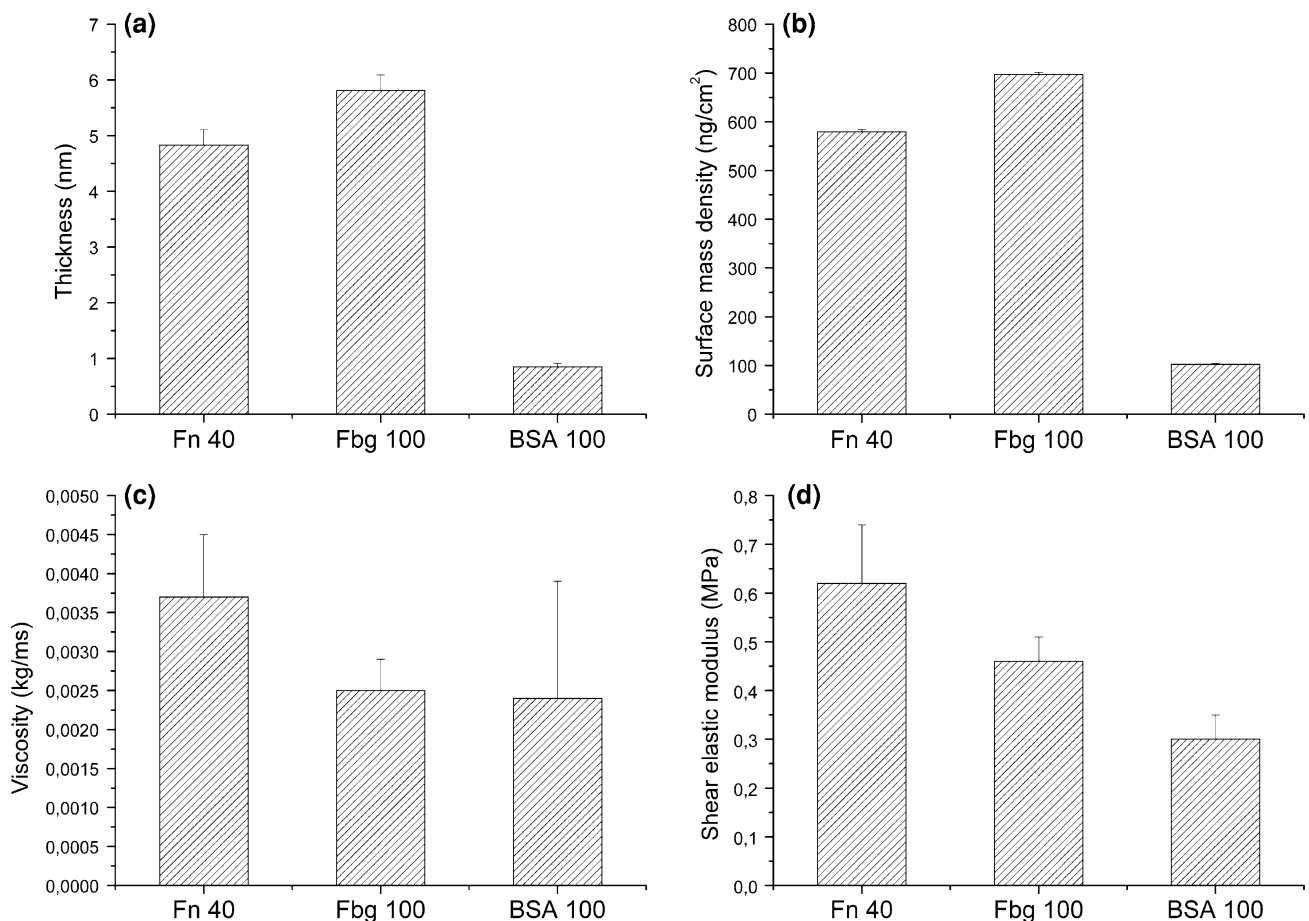


**Fig. 4** **a** Thickness, **b** mass density on surface, **c** viscosity, and **d** shear elastic modulus of adlayers obtained in the experiments shown in Fig. 3. Calculations were performed after 60 min of adsorption time using the Voigt model

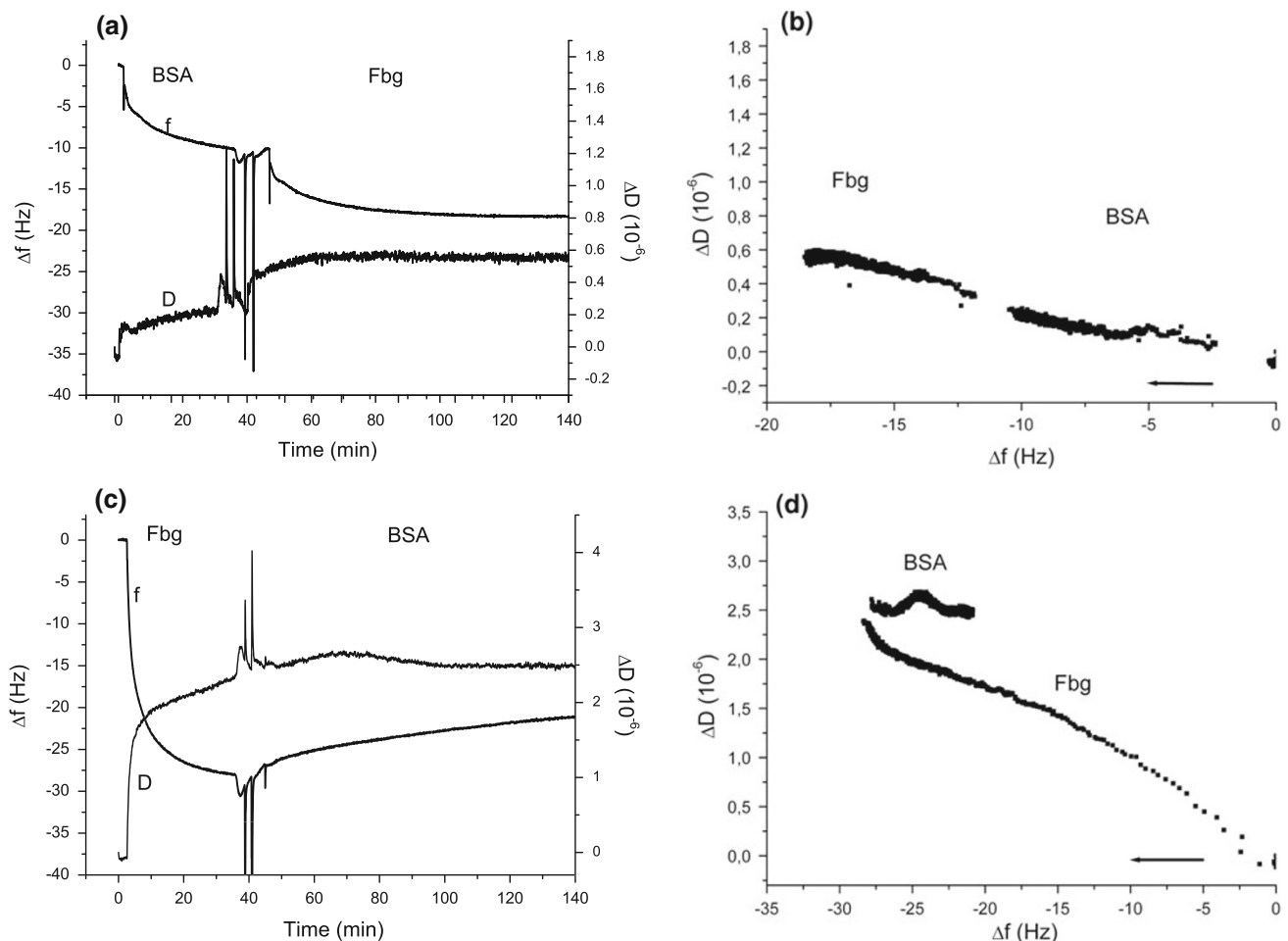


**Fig. 5**  $\Delta f$  and  $\Delta D$  versus time plots (a, c) and  $\Delta D$  versus  $\Delta f$  plots (b, d) for the two-step BSA–Fbg (a, b) and Fbg–BSA (c, d) experiments

mass—as well as a variation of  $\Delta D$  with its maximum reached near after the initiation of the adsorption of BSA.

The first portion of the  $\Delta D$  versus  $\Delta f$  plot for the Fbg–BSA test on  $\text{TiO}_2$ -coated sensors (Fig. 5d) showed a two slope/phase response that was mainly characterized by a significant decrease of the  $\Delta D/\Delta f$  slope in the final part of Fbg adsorption. That was the same response than the one obtained during one-step monoprotein solution studies (Fig. 3). The Fbg-coated  $\text{TiO}_2$ -surfaces were exposed to a BSA solution during the second step of the experiment resulting in a four-stage adsorption process that was ended in a phase of adsorption with steady near-zero  $\Delta D/\Delta f$  slope.

### 3.2.1.1 Interactions Between BSA, Fn and $\text{TiO}_2$ First step: BSA solution–Second step: Fn solution (BSA–Fn).

A rapid decrease in frequency shift was detected during adsorption of the first protein; i.e., BSA (Fig. 6a). During the intermediate step of washing with PBS  $1\times$  certain quantity of BSA desorbed from the adlayer as showed by the slight increase in frequency shift. The notable higher decrease in frequency shift in this BSA–Fn experiment

than in Fbg–BSA and BSA–Fbg experiments can be attributed to the higher concentration of BSA in the solution for this experiment.  $D$  increased with time during BSA adsorption (Fig. 6a). Further adsorption of Fn resulted in both a total frequency shift variation of  $-1$  Hz and an increasing value of the dissipation shift.

The  $\Delta D$  versus  $\Delta f$  plot (Fig. 6b) for the BSA–Fn test showed a single  $\Delta D/\Delta f$  slope/phase process during the initial BSA adsorption. Then, after exposure of the BSA-coated  $\text{TiO}_2$  surfaces to the Fn-solution the adlayer showed an abrupt increase in its  $\Delta D/\Delta f$  slope.

First step: Fn solution–Second step: BSA solution (Fn–BSA).

Figure 6c shows time-resolved frequency and dissipation shift graphs during the two-step Fn–BSA protein adsorption process. During the exposure of BSA to Fn-coated  $\text{TiO}_2$ -surfaces, an increase of 2 Hz in frequency was assessed. The increase in frequency was due to a loss of mass from the protein-coated surface. Interestingly, this was coupled to a continuous slight decrease in dissipation shift.

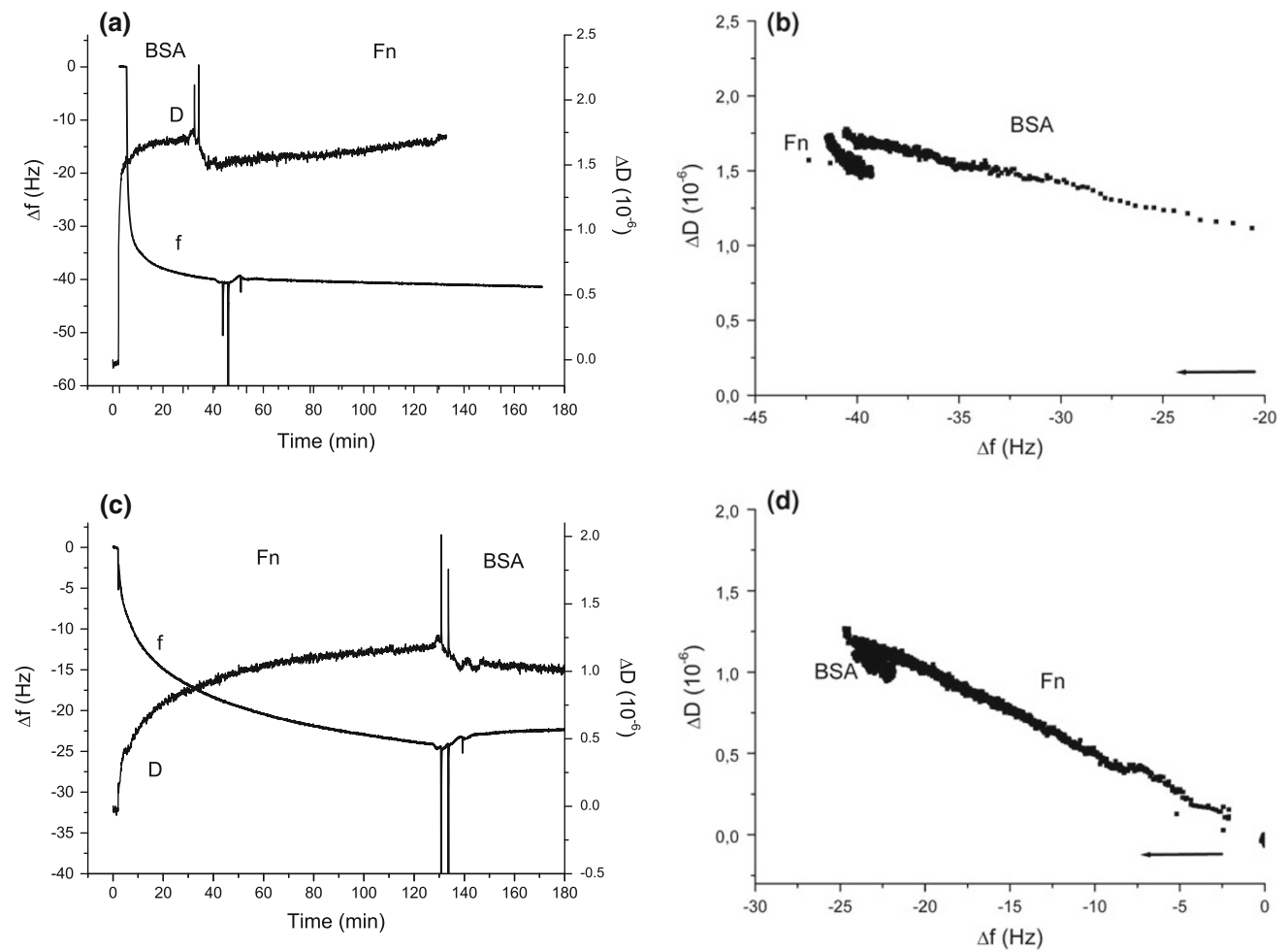


**Fig. 6**  $\Delta f$  and  $\Delta D$  versus time plots (a, c) and  $\Delta D$  versus  $\Delta f$  plots (b, d) for the two-step BSA-Fn (a, b) and Fn-BSA (c, d) experiments

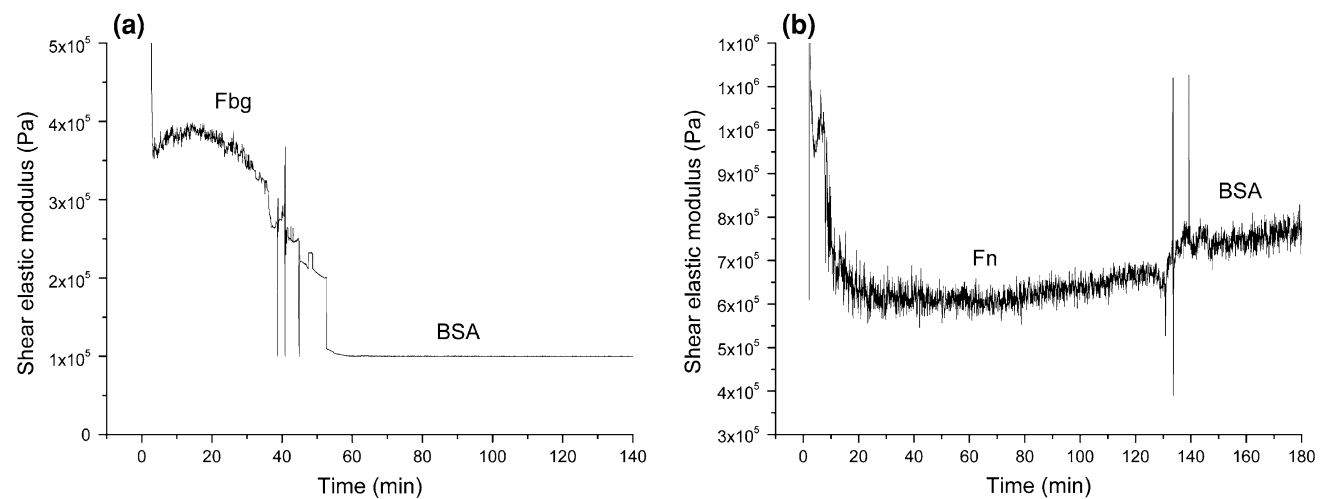


**Fig. 7** Shear elastic modulus of the layer of proteins adsorbed on  $\text{TiO}_2$ -coated sensors during the two-step experiments where BSA was introduced in the system in the second step, **a** Fbg-BSA experiment, **b** Fn-BSA experiment

Figure 6d shows  $\Delta D$  versus  $\Delta f$  plots for the two-step Fn-BSA tests. A constant  $\Delta D/\Delta f$  slope was recorded during the Fn adsorption as it was the case during the one-

step monoprotein adsorption experiments (Fig. 3). The further adsorption of BSA slightly increased the  $\Delta D/\Delta f$  slope.

Figure 7 shows the evolution of the shear elastic modulus comparing the change in rigidity of the resulting protein layer when Fbg (Fig. 7a) or Fn (Fig. 7b) were the first protein to be introduced in the system in the two-step competition experiments. When BSA was introduced in the system after Fn the resulting layer was increasingly more rigid; however, a sudden notable drop in rigidity was recorded when BSA interacted with the previously adsorbed Fbg layer.

## 4 Discussion

### 4.1 Single-Protein Adsorption Studies

Protein concentration in solution and molecular weight of the molecule tested are two of the most influencing properties on mass and thickness of protein adlayers. Other properties, such as protein conformation when adsorbed on the surface and amount of trapped water into the adlayer may also have an important effect on the specific characteristics of the layer of proteins obtained. Our results confirmed previous findings by others [9]: the higher the protein concentration in solution the higher the amount of adsorbed proteins on the surface (Fig. 2a, b).

As previously discussed, the Sauerbrey equation—Eq. 1—provides an accurate estimation of the adsorbed mass only if the adsorbed protein layer on the studied surface is rigid. To determine which model, Sauerbrey or Voigt, is the most appropriate for assessing properties of the protein layer, the frequency and the dissipation shift versus time of the different overtones should be plotted (data not shown). The data will require viscoelastic modelling if  $D$  values are not close to zero, or if  $D$ -shifts (in  $1E-6$ ) are higher than 5 % of  $f$  shifts (in Hz). In addition, if there are significant differences between overtones viscoelastic modelling is suggested [47]. The significant  $\Delta D$  recorded for all the performed tests here indicated that a viscoelastic layer was obtained and thus, the use of the Sauerbrey equation would underestimate the thickness of the protein adlayers on the  $TiO_2$  surfaces. Subsequently, the Voigt model was used to calculate, compare, and discuss the parameters of the protein layers obtained—thickness, viscosity and shear elastic modulus. In addition, surface mass density was calculated from the thickness values using the Voigt model as well.

Fn is a relatively big protein with a molecular weight of 450–500 kDa which is higher than the one of Fbg, 340 kDa. One would expect that the surface mass density for the adsorbed layers from Fn solutions would be higher than those obtained for Fbg layers. This is not the case as shown in Fig. 4b. The higher concentration of Fbg in solution, 100  $\mu\text{g}/\text{m}$ , than the one for the Fn solution, 40  $\mu\text{g}/$

ml, may explain the higher thickness of the Fbg layer. However, we obtained Fbg layers with lower viscosity and shear elastic modulus than the Fn layers (Fig. 4), which is an indication of a less compact Fbg layer in comparison with the Fn layer. The later might be associated to the effect of a protein rearrangement in the layer or to an increased amount of trapped water until the layer is saturated and the change in dissipation is almost constant (Fig. 3). This was further confirmed by the fact that the shear elastic modulus of the layer of Fbg adsorbed from the lower concentration solution, 80  $\mu\text{g}/\text{ml}$ , was higher than the one from the higher concentration solution, 100  $\mu\text{g}/\text{ml}$  (data not shown).

A complex relationship between all these properties could be speculated as further analysis of BSA adsorption was performed. During BSA adsorption, water was continuously being incorporated and trapped in the layer of proteins, as seen in the increasing  $\Delta D$  in Fig. 3 and demonstrated by low values of shear elastic modulus (Fig. 4d). However, the thickness and surface mass density obtained for the BSA-adsorbed layer were significantly lower than for both Fn- and Fbg-adsorbed layers. From those results when comparing with the other types of proteins tested a prevalent influence of the molecular weight (66 kDa), size, and globular-like shape of albumin is suggested. Roach et al. [51] concluded that BSA adsorbs on hydrophilic and hydrophobic surfaces with minimal conformational changes. Thus, the three slopes/phases obtained for BSA adsorption (Fig. 3) might be due to a process of multilayer adsorption, as once demonstrated by Höök et al. [52] studying haemoglobin adsorption on gold-coated sensors.

### 4.2 Two-Step Protein Adsorption Studies

For all the sequential protein adsorption experiments, the adsorption response of the proteins for the first solution introduced in the system was similar to that obtained for single-protein adsorption studies on  $TiO_2$ -surfaces. If differences were found, those were mainly attributed to the different protein concentrations in solution used for the single-protein and two-step studies. Macromolecules that are being adsorbed on a surface can use several adsorption sites depending on their structure and molecular mass. At low concentrations, adsorbed proteins are in an unfolded state with more located binding sites to adsorb [53]. Protein adsorption, such as Fn and human serum albumin [27, 54] are related to structural rearrangements in the molecules that enable them to overcome the unfavourable conditions offered by an electrostatic repelling surface. At higher protein concentrations the adsorption layer becomes more compressed and molecules with different degrees of unfolding will coexist at the interface [55], which makes more difficult for some molecules to overcome the

unfavourable conditions to reach adsorption. This fact can explain the higher rigidity of the protein layer obtained for the lowest Fn and BSA concentrations since protein molecules could be more tightly bound to the surface. The opposite occurred when testing at a higher protein concentration, as the 2 mg/ml BSA concentration used for two-step studies (BSA–Fn). A more viscoelastic protein layer was obtained in comparison with 500  $\mu\text{g/ml}$  (BSA–Fbg) and 100  $\mu\text{g/ml}$  (monoprotein solution studies) BSA concentrations (results not shown).

#### 4.2.1 Interactions Between BSA and Fbg on $\text{TiO}_2$

After the initial adsorption of BSA on  $\text{TiO}_2$ -coated sensors Fbg adsorbed on the  $\text{TiO}_2$ -BSA surface as indicated by the continuous decrease in frequency. The frequency shift following Fbg adsorption was approx.  $-10$  Hz lower than during the monoprotein solution test (Fig. 2). BSA had a high affinity for the  $\text{TiO}_2$ -crystal surfaces which resulted in adsorption of Fbg either on top of BSA-layer or on the few BSA-free available spaces on those crystals. In any case, that resulted in reduced Fbg adsorption on top of the BSA-coated surfaces in comparison with the monoprotein solution test where Fbg interacted directly on top of the  $\text{TiO}_2$  surface. Additionally, this sequence of protein interactions did not change the structural and/or water entrapped in the BSA and Fbg adlayers in comparison with the same protein layers from separated monoprotein solution experiments, as shown in  $\Delta D$ – $\Delta f$  plots (Figs. 5b, 3, respectively). This suggested that a multilayered coating with minimal BSA–Fbg interaction was obtained, i.e. Fbg did not displace, but rather layered on top of the BSA layer.

The interaction processes between these two proteins were different when Fbg was first adsorbed on  $\text{TiO}_2$ -surfaces followed by BSA adsorption (Fig. 5c, d) in comparison with the initial adsorption of BSA followed by Fbg adsorption. Most notably, an increase in frequency shift was recorded after the BSA solution was introduced in the system and interacted with the already formed Fbg-layer on  $\text{TiO}_2$ -crystals. This indicated that BSA was able to displace some of the Fbg molecules that were previously adsorbed on the surfaces. In fact, some previously reported works have concluded that some proteins can displace pre-adsorbed molecules because they have a superior affinity and they are able to bind strongly with the analyzed surface [56]. Although others have shown that BSA has not strong affinity for surfaces with contact angles comparable to those of the  $\text{TiO}_2$ -sensors tested here [51], the small size of BSA can favour this molecule to reach some of the non-covered surface points as well as to compete with Fbg molecules for the already occupied positions on the crystals. If this is the case, BSA molecules showed a higher affinity for  $\text{TiO}_2$  surfaces than Fbg molecules. This

conclusion is aligned with the results discussed in the previous paragraph; i.e., BSA formed a stable layer on the  $\text{TiO}_2$  surfaces that was not disturbed by the later presence of Fbg in solution. The transition stage resulting from the PBS washings after Fbg was adsorbed also indicated that a small percentage of the adsorbed Fbg molecules were removed—those that were only weakly adsorbed to the surface, as exemplified by an increase of the frequency shift and  $\Delta D/\Delta f$  slope before BSA was further introduced in the system. Thus, the displacement of Fbg molecules by BSA molecules can be also favoured by a stronger affinity of the BSA protein to the  $\text{TiO}_2$ -surfaces than Fbg for this system. During the subsequent BSA adsorption, the mechanical properties of the layer significantly dropped (Fig. 7) and some structural rearrangements might have occurred, as shown in Fig. 5d but those potential structural changes of the layer did not notably affect the shear elastic modulus of the overall protein coating (Fig. 7). That confirmed that the mechanical properties of the final coating were mainly determined by the properties of the adsorbed BSA layer and thus, strongly influenced by a significant displacement of the Fbg molecules.

#### 4.2.2 Interactions Between BSA, Fn and $\text{TiO}_2$

The two-step sequential protein adsorption during the BSA–Fn experiments showed a rapid and dramatic decrease in frequency when BSA is introduced in the system, mainly due to its high concentration in PBS. Note that the concentration is 4 times higher than the one used for the BSA–Fbg experiments. Since the solution had an elevated concentration many molecules were attached immediately on the surface. Ramsden [15] concluded that depending on the protein, surface, and solution conditions the occupied area per adsorbed molecules is inversely proportional to the rate the proteins reach the surface. Thus, the rapid BSA adsorption most-likely caused a nearly non-spread molecules layer onto the surface. This was further confirmed by the significant desorption of BSA molecules when the surfaces were washed with PBS that in turn, made the BSA adlayer more rigid, as shown by a decreased dissipation factor. This was an occurrence that did not happen when the BSA–Fbg system was tested. A slight decrease in the frequency shift was recorded during further interaction of Fn with the BSA-layer adsorbed on  $\text{TiO}_2$ -crystals. Thus, Fn is being adsorbed on top of the surface but in a very small quantity. In fact, an almost negligible 1 %-increase in both thickness and surface mass density of the adlayer was calculated after adsorption of Fn. The adsorption of Fn on top of the BSA layer also resulted in a less rigid, less viscous layer with a similar  $\Delta D/\Delta f$  plot than the one obtained during the monoprotein Fn solution test. This, as aforementioned for the BSA/Fbg

experiments, indicated that minimal interaction between the two types of proteins resulted in a multilayered coating.

Again, as in the case of the interaction with Fbg, when BSA was introduced in the second solution during the Fn–BSA two-step sequential adsorption experiments, an increase of frequency shift was recorded, i.e. the coating decreased in total mass. In this case, though, a continuous decrease in dissipation shift during the adsorption of BSA was determined. That indicated that some of the Fn molecules were displaced by BSA molecules with the displacement interactions resulting in a reduced thickness and surface mass density, and an increased rigidity of the resulting adlayer (Fig. 7).

All the previously discussed results showed on the one hand the ability of BSA to compete for locations to be adsorbed and finally displace bigger proteins that were previously adsorbed on the TiO<sub>2</sub>-coated sensors and thus, demonstrated that BSA has a higher affinity for TiO<sub>2</sub> surfaces than Fn and Fbg. On the other hand, BSA adsorption had different effects on the structure and mechanical properties of the resulting layer when Fn or Fbg were pre-adsorbed on the TiO<sub>2</sub>-surfaces as demonstrated by the significant differences found in the effects on the mechanical properties of the final adlayer.

The ‘Vroman effect’ relates to the competition between two or more proteins for the same adsorbent surface. The generalized Vroman effect [57] demonstrated that adsorption from blood plasma involves a complex series of adsorption and displacement steps in which low molecular weight, MW, proteins arriving first at a surface are displaced by relatively higher MW proteins arriving later. Literature has not consistently supported the Vroman effect theory, though. Brash and Lyman [58] proposed that in protein mixtures, such as blood, the proteins would simply adsorb in proportion to their concentrations in solution. Noh et al. [59] agreed with Brash and Lyman’s conclusion, except when mass balance mandates a discrimination against larger proteins adsorbing from a mixture of smaller-and-larger proteins.

Concerning to our results, the studied Fbg/BSA and Fn/BSA experiments showed that BSA displaced larger proteins such as Fn and Fbg whereas in BSA/Fbg and BSA/Fn the larger proteins laid on top of BSA forming an adsorbed protein bi-layer. Overall, we can conclude that in the system studied here (Fn, Fbg, BSA on TiO<sub>2</sub>) the Brash and Lyman effect prevailed since a lower molecular weight and more concentrated protein in solution adsorbed preferentially to TiO<sub>2</sub> surfaces.

**Acknowledgments** This work was supported by the CICYT-Interministerial Commission of Science and Technology of the Ministry of Science and Technology of Spain, Grant MAT2009-13547. The authors thank Dr. Elisabeth Engel and Dr. George Altankov for experimental help with protein solution preparation. MP would like to

thank the Universitat Politècnica de Catalunya (UPC) for funding through a fellowship Grant to complete her PhD graduate studies.

**Open Access** This article is distributed under the terms of the Creative Commons Attribution License which permits any use, distribution, and reproduction in any medium, provided the original author(s) and the source are credited.

## References

- MacDonald DE, Deo N, Markovic B, Stranick M, Somasundaran P (2002) *Biomaterials* 23:1269–1279
- Puleo DA, Nanci A (1999) *Biomaterials* 20:2311–2321
- Andrade JD, Hlady V (1986) *Adv Polym Sci* 79:1–63
- Rabe M, Verdes D, Seeger S (2011) *Adv Colloid Interface Sci* 162:87–106
- Haynes CA, Norde W (1994) *Colloids Surf B Biointerfaces* 2:517–566
- Haynes CA, Sliwinsky E, Norde W (1994) *J Colloid Interface Sci* 164:394–409
- Deligianni DD, Katsala N, Ladas S, Sotiropoulou D, Amedee J, Missirlis YF (2001) *Biomaterials* 22:1241–1251
- Michael K, Vernekar V, Keselowsky B, Meredith J, Latour R, Garcia AJ (2003) *Langmuir* 19:8033–8040
- Schmidt DR, Waldeck H, Kao WJ (2009) Protein adsorption to biomaterials. In: Puleo DA, Bizios R (eds) *Biological interactions on materials surfaces*. Springer, Berlin, pp 2–17
- Béguin S, Kumar R (1997) *Thromb Haemost* 78:590–594
- Kumar R, Béguin S, Hemker HC (1994) *Thromb Haemost* 72:713–721
- Tzoneva R, Heuchel M, Groth T, Altankov G, Albrecht W, Paul D (2002) *J Biomater Sci Polym Ed* 13:1033–1050
- Scotchford CA, Ball M, Winkelmann M, Voros J, Csucs C, Brunette DM, Danuser G, Textor M (2003) *Biomaterials* 24:1147–1158
- Renner L, Pompe T, Salchert K, Werner C (2005) *Langmuir* 21:4571–4577
- Ramsden JJ (1994) *Q Rev Biophys* 27:41–105
- Smith RA, Mosesson MW, Daniels AW, Kent T (2000) *J Mater Sci Mater Med* 11:279–285
- Sivaraman B, Latour RA (2010) *Biomaterials* 31:1036–1044
- Godek ML, Michel R, Chamberlain LM, Castner DG, Grainger DW (2009) *J Biomed Mater Res Part A* 88A:503–519
- Williams DF (1976) Corrosion of implant materials. *Annu Rev Mater Sci* 6:237–266
- Liu XY, Chu PK, Ding CX (2004) *Mater Sci Eng R Rep* 47:49–121
- Textor M, Sittig C, Frauchiger V, Tosatti S (2001) Properties and biological significance of natural oxide films on titanium and its alloys. In: Brunette DM, Tengvall P, Textor M, Thomsen P (eds) *Titanium in medicine*. Springer, Berlin, pp 172–224
- Lausmaa J (1996) *J Electron Spectrosc Relat Phenom* 81:343–361
- Wälivaara B, Aronsson B, Rodahl M, Lausmaa J, Tengvall P (1994) *Biomaterials* 15:827–834
- Paine M, Wong J (2003) Osteoblast response to pure titanium and titanium alloy. In: Ellingsen J, Lyngstadaas S (eds) *Bio-implant interface. Improving biomaterials and tissue reactions*. CRC Press, Boca Raton
- Holgers K-M, Esposito M, Kalltorp M, Thomsen P (2001) Titanium in soft tissues. In: Brunette DM, Tengvall P, Textor M, Thomsen P (eds) *Titanium in Medicine*. Springer, Berlin, pp 513–560

26. Tengvall P (2001) Proteins at titanium interfaces. In: Brunette DM, Tengvall P, Textor M, Thomsen P (eds) *Titanium in Medicine*. Springer, Berlin, pp 457–484
27. Sousa SR, Moradas-Ferreira P, Barbosa MA (2005) *J Mater Sci Mater Med* 16:1173–1178
28. MacDonald DE, Markovic B, Boskey AL, Somasundaran P (1998) *Colloids Surf B Biointerfaces* 11:131–139
29. Norde W, Lyklema J (1978) *J Colloid Interface Sci* 66:257–265
30. Voinova M, Rodahl M, Jonson M, Kasemo B (1999) *Phys Scr* 59:391–396
31. Hook F, Kasemo B, Nylander T, Fant C, Sott K, Elwing H (2001) *Anal Chem* 73:5796–5804
32. Hook F, Voros J, Rodahl M, Kurrat R, Boni P, Ramsden JJ, Textor M, Spencer ND, Tengvall P, Gold J, Kasemo B (2002) *Colloids Surf B Biointerfaces* 24:155–170
33. Hook F, Rodahl M, Brzezinski P, Kasemo B (1998) *Langmuir* 14:729–734
34. Geometrical Product Specifications (GPS)—Surface texture: Profile method—Metrological characteristics of phase correct filters. ISO 11562:1996. 1996. Ref Type: Generic
35. Wassell DT, Embery G (1996) *Biomaterials* 17:859–864
36. MacDonald DE, Markovic B, Allen M, Somasundaran P, Boskey AL (1998) *J Biomed Mater Res* 41:120–130
37. Tamada Y, Ikada Y (1993) *J Colloid Interface Sci* 155:334–339
38. Bai Z, Filiaggi MJ, Dahn JR (2009) *Surf Sci* 603:839–846
39. Grunkemeier JM, Tsai WB, McFarland CD, Horbett TA (2000) *Biomaterials* 21:2243–2252
40. Oliva F, Avalle L, Cámara O, De Pauli C (2003) *J Colloid Interface Sci* 261:299–311
41. Andersson M, Andersson J, Sellborn A, Berglin M, Nilsson B, Elwing H (2005) *Biosens Bioelectron* 21:79–86
42. Thompson M, Arthur CL, Dhaliwal GK (1986) *Anal Chem* 58:1206–1209
43. Fredriksson C, Kihlman S, Rodahl M, Kasemo B (1998) *Langmuir* 14:248–251
44. Hemmersam AG, Foss M, Chevallier J, Besenbacher F (2005) *Colloids Surf B Biointerfaces* 43:208–215
45. Ward MD, Buttry DA (1990) *Science* 249:1000–1007
46. Rodahl M, Hook F, Krozer A, Brzezinski P, Kasemo B (1995) *Rev Sci Instrum* 66:3924–3930
47. Q-Sense. QCM-D. 2008. <http://www.q-sense.com/>. Accessed 21 February 2008
48. Weber N, Pesnell A, Bolikal D, Zeltinger J, Kohn J (2007) *Langmuir* 23:3298–3304
49. Hovgaard M, Rechendorff K, Chevallier J, Foss M, Besenbacher F (2008) *J Phys Chem B* 112:8241–8249
50. Vörös J (2004) *Biophys J* 87:553–561
51. Roach P, Farrar D, Perry CC (2005) *J Am Chem Soc* 127:8168–8173
52. Hook F, Rodahl M, Kasemo B, Brzezinski P (1998) *Proc Nat Acad Sci USA* 95:12271–12276
53. Yang YZ, Cavin R, Ong JL (2003) *J Biomed Mater Res Part A* 67A:344–349
54. do Serro APVA, Fernandes AC, Saramago BDV, Norde W (1999) *J Biomed Mater Res* 46:376–381
55. Miller R, Treppo S, Voigt A, Zingg W, Neumann AW (1993) *Colloids Surf* 69:203–208
56. Jung S, Lim S, Albertorio F, Kim G, Gurau MC, Yang RD (2003) *J Am Chem Soc* 125:12782–12786
57. Vroman L, Adams AL (1969) *Surf Sci* 16:438–446
58. Brash JL, Lyman DJ (1969) *J Biomed Mater Res Part A* 3:175–189
59. Noh H, Vogler EA (2007) *Biomaterials* 28:405–422